



# Homogeneous ice nucleation rate at negative pressures: The role of the density anomaly

Elise Rosky <sup>a</sup>, Will Cantrell <sup>a</sup>, Tianshu Li <sup>b</sup>, Raymond A. Shaw <sup>a,\*</sup>

<sup>a</sup> Department of Physics, Michigan Technological University, 1400 Townsend Dr, Houghton, 49931 MI, United States

<sup>b</sup> Department of Civil & Environmental Engineering, George Washington University, 800 22nd Street, NW, Washington, DC 20052, United States



## ARTICLE INFO

### Keywords:

Homogeneous nucleation  
Ice nucleation  
Pressure dependence of nucleation  
Molecular dynamics

## ABSTRACT

Recent experiments suggest a role for pressure fluctuations in nucleation. Homogeneous ice nucleation rates for the ML-mW and mW water models are evaluated at pressures ranging from atmospheric to  $\sim 1000$  atm, using forward flux sampling and constant cooling simulations. Results indicate that the density difference  $\Delta\nu_{ls}$  between water and ice exhibited by these models plays a central role in controlling the change in nucleation rate with pressure. A linear function is found to be a reasonable approximation for lines of constant nucleation rate, which can be useful in making experimental predictions to advance the study of ice nucleation mechanisms.

## 1. Introduction

The physics governing the phase transition from liquid water to ice is still under investigation. Molecular dynamics (MD) simulations of ice nucleation on the molecular scale are helpful in revealing the fundamental mechanisms involved in ice formation. This topic is relevant to understanding ice formation in clouds, and efforts to control freezing through enhancing or suppressing ice nucleation [1,2]. Homogeneous ice nucleation occurs in supercooled water when an ice cluster of critical radius forms, overcoming the Gibbs free energy barrier imposed by the surface energy of the cluster, without catalysis from any impurities or container walls. The ice nucleation rate coefficient,  $J$ , is the number of critical clusters forming per unit volume and time. The nucleation rate increases as the temperature is lowered further from the melting point. In this study, we aim to understand how negative pressures (negative valued diagonal components of the stress tensor) within the liquid influence ice nucleation rates.

Experiments and everyday experience show that various processes can help supercooled liquid overcome the free energy barrier and catalyze ice nucleation. Introducing certain impurities, or shaking or agitating the water are examples [3,4]. The explanation for the latter observations is still unclear. In controlled lab experiments, only certain types of mechanical agitation are effective at catalyzing ice formation [5,6]. Experiments show that moving the contact line of a water droplet across its substrate only triggers ice nucleation when combined with stretching/distorting of the contact line [7]. This finding indicates that

the water surface plays an important role and points to a possible contribution from Laplace pressure, which arises from curved liquid-vapor interfaces. A concave surface has a negative radius of curvature and results in negative Laplace pressure. Just as the melting temperature of water increases under negative pressures [8], ice nucleation rates also increase due to a lowering of the Gibbs free energy barrier. Therefore, it's possible that negative pressure/stress perturbations imposed on a supercooled liquid droplet can increase the ice nucleation rate while maintaining a constant temperature. This and other possible sources of negative pressure in atmospheric water droplets are discussed in Marcolli et al. [9] and Yang et al. [10]. The atmospheric science community has been predominately focused on the temperature dependence of ice nucleation. This work, in contrast, is another step in exploring the role that pressure changes might play.

We use molecular dynamics to explore the relative roles of temperature and pressure on ice nucleation; specifically, for the range of pressures expected in experimental and atmospheric scenarios [10]. Li et al. [11], Yang et al. [5], and others have proposed that a Clausius-Clapeyron-like relation can be used to express the equivalence between temperature and pressure in achieving a given nucleation rate:

$$p(T) = p_0 + \frac{l_f}{T_m \Delta \nu_{ls}} (T - T_0), \quad (1)$$

where  $p_0$  and  $T_0$  are known reference pressure and temperature values for a nucleation rate coefficient of interest. In this study we take atmospheric pressure as the reference. The molar volume difference between

\* Corresponding author.

E-mail addresses: [emrosky@mtu.edu](mailto:emrosky@mtu.edu) (E. Rosky), [rashaw@mtu.edu](mailto:rashaw@mtu.edu) (R.A. Shaw).

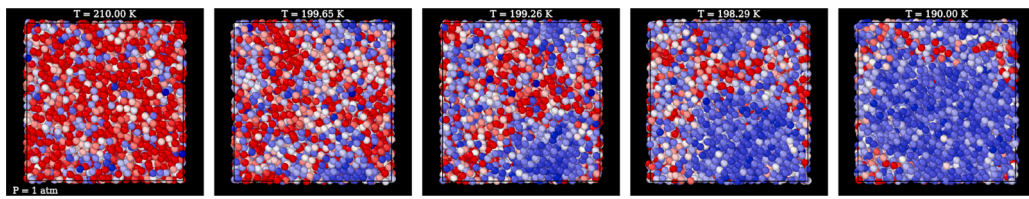


**Fig. 1.** Snapshots from a representative constant cooling simulation where homogeneous freezing occurs in the mW model. The coloring indicates the value of the  $q_6$  order parameter, with blue shades denoting molecules with ice-like  $q_6$  order parameter greater than 0.54 and red shades denoting liquid-like order parameter.

liquid and ice,  $\Delta v_{ls}$ , is negative in the pressure regime considered in this study, a phenomenon known as the water density anomaly. The variable  $l_f$  is the latent heat of fusion and  $T_m$  is the melting temperature, both at  $p_0$ . In subsequent sections, we will outline the derivation of this approximation and evaluate the extent to which it provides a reasonable prediction of the nucleation rate in pressure–temperature coordinates.

Freezing of water at negative pressures lacks both simulated and experimental data. Roedder [8] took measurements of the melting temperature of water at negative pressures, but to our knowledge, no experimental assessment of homogeneous freezing rates at negative pressures has been conducted. Evidence for an increase in ice nucleation rates at negative pressures is found by extrapolating experimental data at positive pressures into the negative pressure regime [9], and is also implied by the pressure and temperature dependence of the Gibbs free energy barrier in classical nucleation theory (CNT). A recent study by Bianco et al. used molecular dynamics simulations to explore ice nucleation rates in the TIP4P/Ice water model at negative pressures [12]. Their work explores anomalous behaviors that occur in water in the negative pressure regime, and reports nucleation rates using seeding, an approximate method that produces rigorous results by combining molecular dynamics simulations with CNT.

In this study, we consider two coarse-grained water models that are commonly used to explore ice nucleation due to their computational efficiency: ML-mW and the original mW model. The mW model was introduced by Molinero et al. [13] based on the Stillinger–Weber potential. The ML-mW model was created by further optimizing the mW model parameters using machine learning with properties of real water as a target [14]. If the approximation given by Eq. 1 is valid, it suggests the density anomaly plays a central role in determining the slope of lines of constant nucleation rate in pressure–temperature space. The molar volume difference upon melting,  $\Delta v_{ls}$ , has undergone great improvement in the ML-mW model compared to the original mW model. The experimental value for  $\Delta v_{ls}$  at 1 atm and 273 K is  $-1.61 \text{ cm}^3 \text{ mol}^{-1}$ , which the ML-mW model reproduces with much more fidelity than the original mW model, giving  $-1.38$  and  $-0.42$  respectively [14]. These two water models, which exhibit significantly different density anomalies, provide useful contrasts to assess the validity of Eq. 1 and explore the dependence of nucleation rates on pressure. We propose that the improvement to  $\Delta v_{ls}$  results in a more accurate representation of the homogeneous freezing line,  $(dp/dT)_{J=\text{const.}}$ .

## 2. Methods and Results

We investigate the homogeneous ice nucleation rate coefficients of the mW and ML-mW water models at 1,  $-500$ , and  $-1000$  atm. Most studies of ice nucleation and water model properties have been conducted at 1 atm, so inclusion of this pressure allows us to compare and validate our results with other studies. The  $-500$  atm and  $-1000$  atm values were chosen to be within the negative Laplace pressure range that would correspond to negative surface curvatures down to approximately 10 nm radius, and could account for enhanced nucleation rates observed in experiments [7]. The selected pressures remain in the regime where the molar volume of ice is larger than liquid water,  $\Delta v_{ls} < 0$ . The sign of  $\Delta v_{ls}$  is a crucial factor when studying the behavior of homogeneous freezing with respect to pressure. Bianco et al. [12] shows a peak in the

curve of the homogeneous nucleation rate in TIP4P at around  $-1000$  atm, which is caused by the density anomaly switching sign. In our study, we also notice the density of ice and liquid converging as we approach  $-1000$  atm.

We use two approaches to obtain nucleation rates. In the first method, we obtain nucleation rates from direct simulations of homogeneous ice nucleation at negative pressures. We do this by repeating constant cooling rate simulations many times at a fixed pressure. This approach is akin to experimental methods of measuring ice nucleation rates. The second method obtains nucleation rates in a range of temperatures and (negative) pressures using forward flux sampling [15] at constant temperature. These two approaches are complementary and allow us to explore a broad range of nucleation rates. They are also more direct than the methods commonly used in MD studies, where nucleation rates are derived using precise calculation of thermodynamic properties combined with expressions from classical nucleation theory [12,16]. The methods used in our study do not rely on CNT, thus we are able to compare the results of our simulations with theoretical expressions. In our analysis, we compare the slope of our constant nucleation rate lines with theoretical predictions from Eq. 1.

LAMMPS [17] is used to conduct the molecular dynamics simulations. For the constant cooling rate simulations, a simulation box containing 4,096 coarse-grained water molecules is first equilibrated at the starting temperature. The temperature range that the system is cooled through differs for each pressure and between the models. The temperature range in each case is selected so that ice nucleation is extremely likely to occur during the linear cooling process at the cooling rate chosen. For the mW model the temperature ranges are 215 K to 195 K at 1 atm and  $-500$  atm; and 215 K to 200 K at  $-1000$  atm. For the ML-mW model the ranges are 225 K to 205 K at 1 atm; 230 K to 210 K at  $-500$  atm; and 230 K to 215 K at  $-1000$  atm. The constant cooling rate simulations are conducted in an isenthalpic (NPH) ensemble coupled with a thermostat and with periodic boundary conditions employed. After equilibration at the initial temperature, the system is cooled at rate of 0.25 K/ns. Johnston et al. reported that a cooling rate of 1 K/ns is the highest cooling rate one can use to still observe crystallization in mW model nanodroplets containing 13,824 molecules [18]. We found that at lower pressures, e.g.,  $-1000$  atm, lower cooling rates were needed to observe crystallization. For the ML-mW, 16% of our trajectories at  $-1000$  atm did not crystallize. This is marked by a very gradual, linear increase in ice-like fraction during cooling with the final ice fraction not reaching 0.8. These runs were not included in the data on ice nucleation phase transition.

The phase of the system is monitored using the  $q_6$  order parameter with a cutoff distance of 3.5 Angstroms [19]. Fig. 1 shows how this order parameter evolves for each atom in the volume of water as the system freezes. A molecule with  $q_6$  order parameter greater than 0.54 is considered an ice-like molecule and is colored blue in Fig. 1 while atoms with  $q_6$  value smaller than the 0.54 threshold are considered liquid-like and are shaded in red. This threshold was determined by measuring the distribution of order parameters in a box of pure ice, and selecting a threshold value just outside that range. The threshold we have chosen is the same for both ML-mW and mW models and is consistent with the threshold used in other studies [20]. To determine the freezing temperature of a single cooling run, we look at the ratio of ice-like molecules

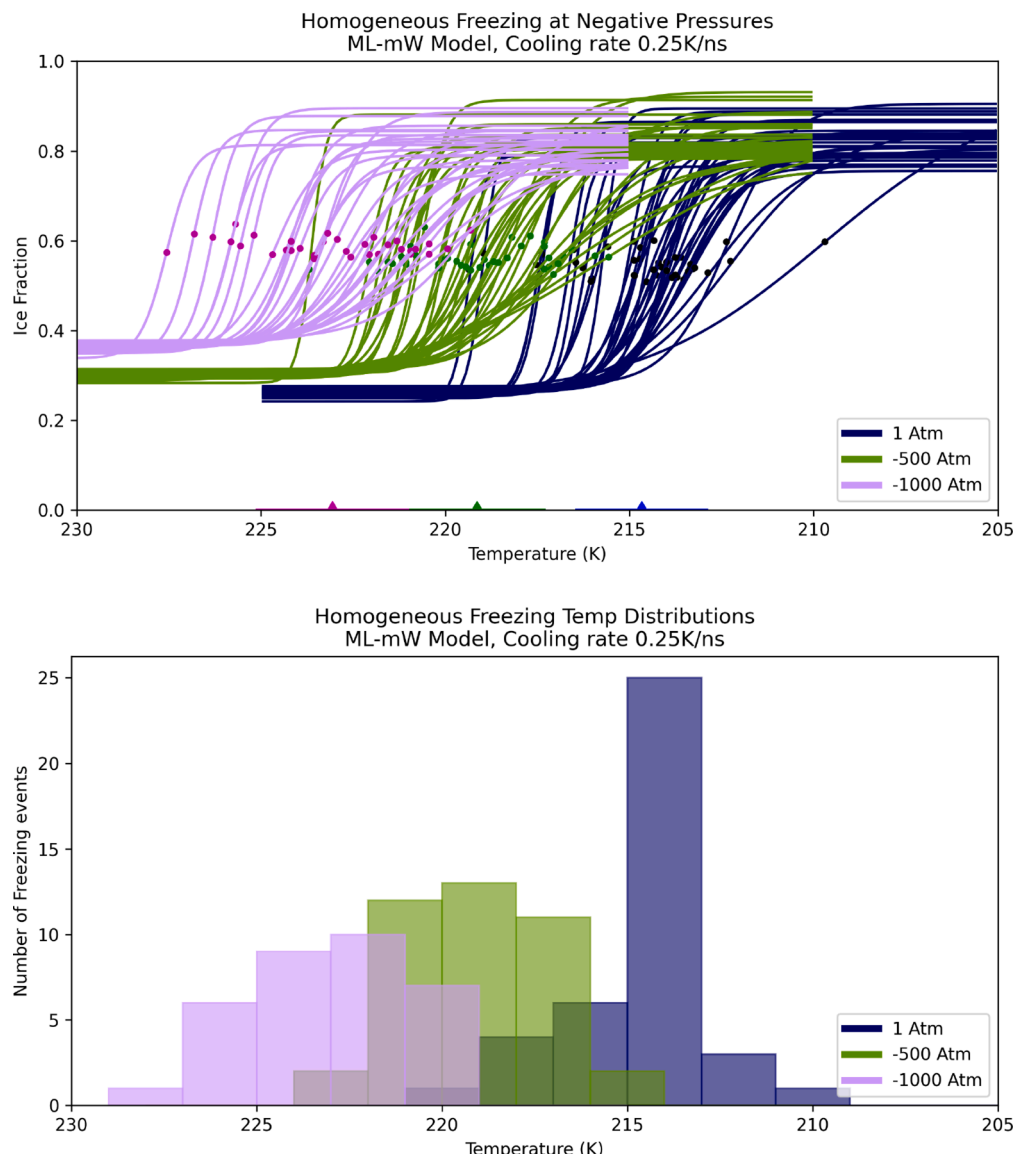


**Fig. 2.** Top: All freezing trajectories for the ML-mW model at three different pressures. The dots indicate the inflection point that is used as the nominal freezing temperature for each run. The markers on the abscissa denote the average freezing temperature for each pressure, and the standard deviation. Bottom: Distribution of nucleation events, used to calculate nucleation rates.

to total molecules as a function of time, which is equivalent to a function of temperature because the system is being cooled at a constant rate. When the system freezes, the fraction of ice-like molecules steeply increases and plateaus at around 0.8. We fit a sigmoidal curve,  $F(t) = A/(1 + \exp(-B(x - C))) - D$ , to the data and specify the freezing temperature to be the inflection point of the sigmoid.  $A, B, C$ , and  $D$  are fitting parameters that represent the maximum ice fraction, speed of transition, inflection point, and vertical shift, respectively. These sigmoidal fits can be seen in the top panel of Fig. 2, which shows all the simulations trajectories for the ML-mW model. At each pressure, 30–50 cooling trials are run to gather a distribution of freezing temperatures, and the resulting temperature distributions are shown in the bottom panel of Fig. 2.

In Chan et al., ML-mW water is cooled at a rate of 0.5 K/ns at 1 atm, and ice nucleation occurs at 210 K [14]. With our slower cooling rate of 0.25 K/ns, we observe that ice nucleation in ML-mW occurs at a higher temperature of 215 K. As anticipated, Fig. 2 shows that homogeneous ice nucleation occurs at higher temperatures when the system is under more negative pressures. This is seen to be the case for both water models, with the ML-mW exhibiting a larger increase than the original mW.

The freezing temperature distributions in the bottom panel of Fig. 2 are used to calculate nucleation rate coefficients in these temperature ranges using the method described by Zobrist et al. [21]. We count the number of freezing events that occur in evenly spaced temperature intervals centered at temperatures  $T_i$ . Next the total observation time in each temperature interval,  $t_{tot,i}$ , is calculated as the sum of the contributions from the simulation trajectories that remained liquid over the entire temperature interval and the ones that freeze. Once a trajectory freezes, the remaining time spent in that temperature interval is not counted in the observation time. We obtain the average homogeneous ice nucleation rates ( $s^{-1}$ ) at the mean temperatures  $T_i$  by dividing the total number of freezing events in the internal by  $t_{tot,i}$ . To obtain the nucleation rate coefficient ( $s^{-1} m^{-3}$ ) from this, we divide by the volume of the simulation box.

The nucleation rate coefficients observed via constant cooling rate simulations are confined to a certain observable range, limited by the chosen cooling rate and volume of water. The calculated nucleation rate coefficients for each pressure are on the order of  $10^{32}$  and  $10^{33} s^{-1} m^{-3}$ , plotted in Fig. 3. This method of cooling a water ‘sample’ many times is similar to the way that freezing temperature measurements are often

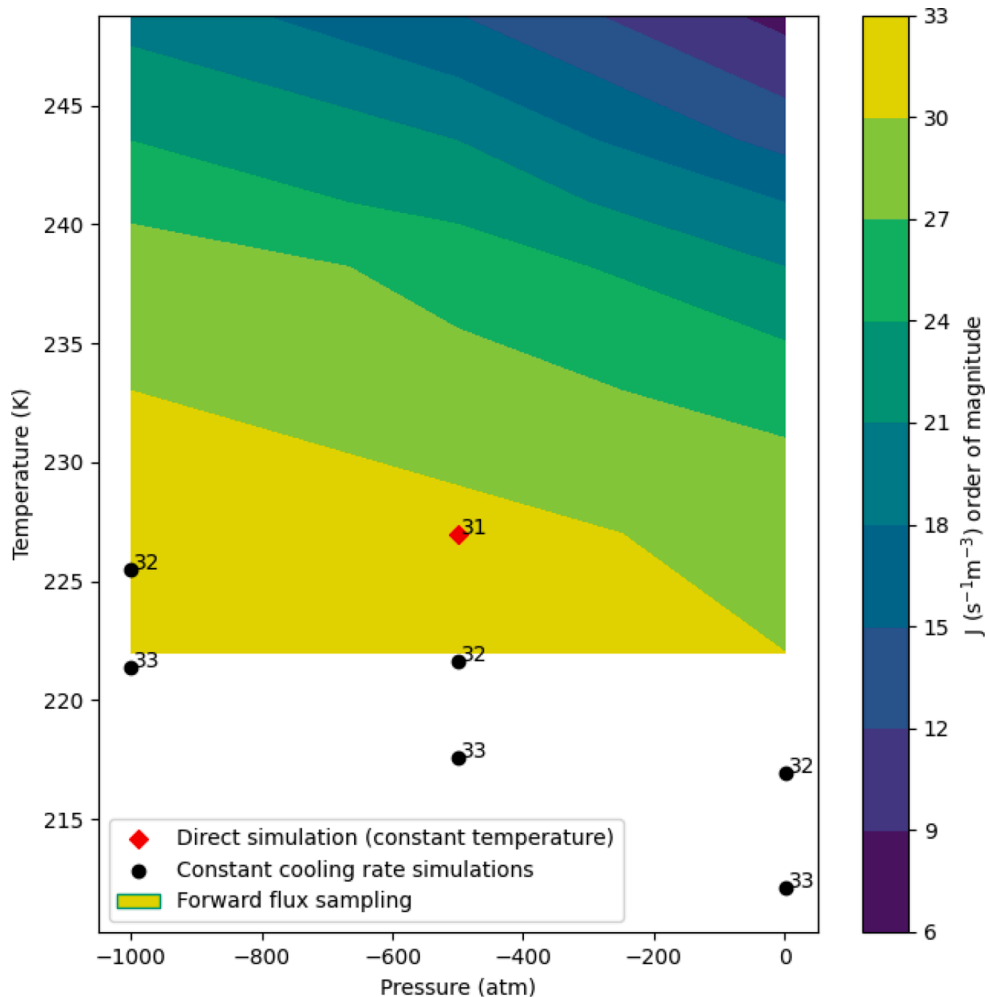


**Fig. 3.** Contours of constant nucleation rate coefficient for the ML-mW model from forward flux sampling simulations. The black points are data from constant cooling rate simulations, labeled with the nucleation rate coefficient order of magnitude. The red data point is from direct MD simulation at constant temperature and pressure. The data sets are self consistent and the contour lines are roughly linear.

conducted experimentally [21–24], albeit that the sample volume in these simulations ( $1.3 \times 10^{-19} \text{ cm}^3$ ) is much smaller than in experiments and the cooling rate is much faster. As a result, the nucleation rate coefficients accessible to this approach falls far beyond experimental range. This gap can be closed by the forward flux sampling approach, as discussed later.

Fig. 4 shows the pressure versus temperature dependence of the  $J = 10^{32} \text{ s}^{-1} \text{ m}^{-3}$  line (triangles) for both the mW and ML-mW models plotted along with the equilibrium melting point line (circles). There is 99% certainty that the  $J = 10^{32} \text{ s}^{-1} \text{ m}^{-3}$  line lies within the shaded region [25].

The data points for the melting-point line are obtained by using the direct-phase coexistence method at each pressure, where the melting temperature is taken as the lowest temperature at which the system completely melts [26,27]. The grey solid line is the experimental melting point line extrapolated to negative pressures [9]. For both models, water melts at higher temperatures when the pressure is negative in accordance with the Clausius–Clapeyron relation. The qualitative behavior of the ML-mW melting point line is in good agreement with the extrapolation from experimental measurements. It is worth noting that the ML-mW melting temperature obtained using this method is greater than what was reported in Chan et al. [14] by 3 K (See A).

To gain a more complete understanding of the  $p, T$  dependence of nucleation rate, we also calculate the nucleation rate coefficients of the ML-mW model for a range of pressures and temperatures using forward

flux sampling (FFS) [15]. FFS enables a direct calculation of nucleation rate coefficient covering a wide range of thermodynamic conditions, particularly those where nucleation rate becomes too small to be obtained by standard MD simulation. More importantly, since FFS does not rely on any nucleation theory, the method can be used independent of CNT. Indeed, FFS has been successfully employed to study homogeneous ice nucleation based on both mW model [28,29] and TIP4P/Ice model [30].

Here we carry out FFS calculation using our recent implementation to compute homogeneous ice nucleation rate coefficients for the  $p, T$  range from  $-1000 \text{ atm}$  to  $1 \text{ atm}$  and  $222 \text{ K}$  to  $250 \text{ K}$ , respectively. Under the framework of FFS [15], the rate constant  $R$  is given by  $R = \dot{\Phi}_{\lambda_0} \prod_{i=0}^n P(\lambda_i | \lambda_{i-1})$ , where  $\dot{\Phi}_{\lambda_0}$  is the flux rate crossing the first interface  $\lambda_0$ , and  $P(\lambda_i | \lambda_{i-1})$  is the probability for a trajectory starting from the interface  $\lambda_{i-1}$  and successfully reaching the next interface  $\lambda_i$ . The interface  $\lambda_i$  is defined by the order parameter  $\lambda$ , which is the number of ice-like water molecules, characterized by a local bond-order parameter  $q_6 > 0.5$ , within the largest ice cluster [28]. For ice nucleation based on the mW model, such an order parameter has been demonstrated to effectively reflect the actual reaction coordinates of ice nucleation [31–33]. Given the similarity between the mW and ML-mW models, we thus expect this order parameter is equally applicable to the current study. The initial flux rate  $\dot{\Phi}_{\lambda_0}$  is obtained through dividing the number  $N$  of direct crossings to the first interface  $\lambda_0$  from liquid basin ( $\sim 200$ ) by the product of the total simulation time  $t$  of this step and the simulation

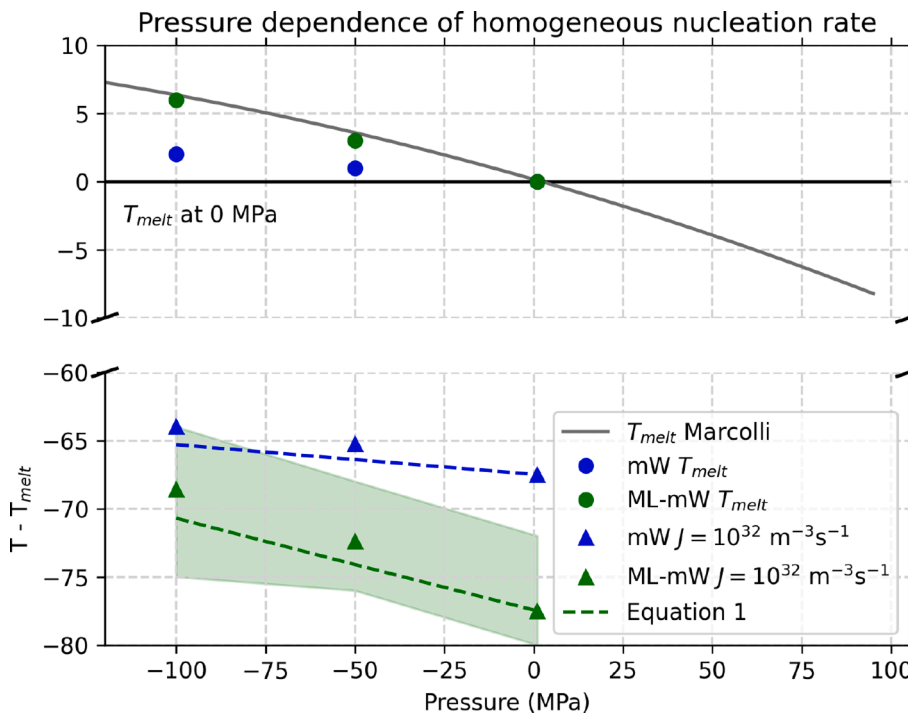


**Fig. 4.** ‘Phase diagram’ showing the pressure and temperature dependence of the equilibrium melting point and line of constant nucleation rate coefficient  $J = 10^{32} \text{ m}^{-3} \text{ s}^{-1}$ . Circles are the melting temperatures for the mW water model (blue) and ML-mW model (green), while the grey line is the experimental melting point line extrapolated to negative pressures [9]. Triangles denote our simulation results for homogeneous nucleation rate coefficient at negative pressures. The dashed lines are theoretical predictions given by Eq. 1. The simulation results obtained at 1 atm are used as the reference values ( $p_0, T_0$ ) for Eq. 1. The origin of the y-axis is set as the melting temperature,  $T_{melt}$  at 1 atm.

volume  $V$ , namely,  $\dot{\Phi}_{\lambda_0} = N/(tV)$ . Using the collected configurations at the interface  $\lambda_0$ , we then consecutively fire a large number of shootings  $M_{i-1}$  at each interface  $\lambda_{i-1}$  and collect  $N_{i-1}$  ( $\sim 120$ ) configurations that successfully cross the next interface  $\lambda_i$ , to compute the crossing probability  $P(\lambda_i|\lambda_{i-1}) = N_{i-1}/M_{i-1}$ . The convergence of the calculation with respect to the number of collected configurations is carefully checked, as explained in B. The typical error bar of the computed nucleation rate coefficient is within 75 ~ 90% of the absolute rate [11]. To further enhance the accuracy of the calculated rate coefficients, we conduct three independent FFS runs for each  $p, T$  condition, through which the final rate is obtained by a geometric average of the calculated rates, i.e.,  $R(p, T) = \left( \prod_{j=1}^3 R_j \right)^{1/3}$ . The FFS calculations cover a wide range of ice nucleation rate coefficients, from  $10^8 \text{ s}^{-1} \text{ m}^{-3}$  to  $10^{33} \text{ s}^{-1} \text{ m}^{-3}$ .

Fig. 3 reports the contours of constant nucleation rate coefficient for ML-mW obtained from FFS, along with data from the constant cooling rate simulations. The two methods show agreement to within the uncertainties. To ensure that FFS and constant cooling rate simulations are consistent with direct MD simulation of homogeneous nucleation at a fixed temperature and pressure, we carried out direct MD simulation for the ML-mW model at  $-500$  atm and  $227$  K, one of few conditions where nucleation is accessible to direct MD. The nucleation rate coefficient at this condition is obtained by 20 independent trajectories through fitting the distribution of induction time following the method in Cox et al. [34] (see B for details.) This data point is plotted on Fig. 3, confirming the self-consistency of our methods.

### 3. Discussion

The performance of the ML-mW model is summarized by Chan et al. [14]. As acknowledged there, the improvement in  $\Delta v_{ls}$  results in an improved representation of the melting point line,  $(dp/dT)_{melt}$  [14]. From the Clausius–Clapeyron relation,  $(dp/dT)_{melt} = \Delta s/\Delta v_{ls}$ , it is clear that the model’s improvement in  $\Delta v_{ls}$  is primarily responsible for the improved behavior. The change in entropy upon melting,  $\Delta s$ , is the same within 5% between the two models, whereas the change in volume upon melting,  $\Delta v_{ls}$ , differs by roughly 230% between the two models. In this study, we analyze our simulation results in the context of Eq. 1, leading

us to conclude that an accurate representation of  $\Delta v_{ls}$  will also result in a more accurate representation of constant homogeneous nucleation rate lines,  $(dp/dT)_{J=const}$ .

When considering the behavior of homogeneous nucleation as a function of negative pressure, we can look at two effects: an elevation of the melting point, and a lowering of the Gibbs free energy barrier to nucleation. If one assumes that the level of supercooling needed to achieve a given nucleation rate coefficient remains fixed as one moves to lower pressures, then the elevated melting point alone leads to an equivalent elevation in the temperature corresponding to a given nucleation rate coefficient. However, the level of supercooling required is also expected to decrease due to a lowering of the Gibbs free energy barrier to nucleation:

$$\Delta G^* = \frac{16\pi\gamma_{ls}^3}{3(\rho\Delta\mu)^2}. \quad (2)$$

In this expression,  $\rho$  is the ice density,  $\gamma_{ls}$  is the solid–liquid interfacial energy, and  $\Delta\mu$  is the change in chemical potential between the solid and liquid. A change in pressure shifts the chemical potential difference  $\Delta\mu$  [35,36]:

$$\Delta\mu = \frac{l_f(T_m - T)}{T_m} + \Delta p \Delta v_{ls}, \quad (3)$$

where  $l_f$  is the enthalpy of fusion and  $T_m$  is the equilibrium melting temperature at the reference pressure,  $p_0$ . A derivation of Eq. 3 is included in C. As long as  $\Delta v_{ls}$  is negative, a decrease in pressure will increase  $\Delta\mu$  at any given temperature, lowering the magnitude of  $G^*$ . This in turn increases the nucleation rate. We note that the value of  $\Delta v_{ls}$  decreases with decreasing pressure and is expected to eventually reach an inflection point where it switches sign [12], so this proposed enhancement in nucleation rate due to  $\Delta v_{ls}$  is confined to the negative-pressure range where  $\Delta v_{ls}$  remains negative, approximately the pressure range of this study.

An approximate expression of this nucleation enhancement with decreasing pressure is proposed by Eq. 1. Its derivation is outlined here, with mathematical details provided in C. Starting from a reference point  $(p_0, T_0)$  with a known nucleation rate coefficient  $J$ , we would like to find

$p, T$  coordinates where this rate coefficient remains constant. By equating  $J(p_0 + \Delta p, T_0 + \Delta T) = J(p_0, T_0)$ , we arrive at an equation for lines of constant  $J$  in terms of pressure and temperature. When applying the approximation that  $(T_0 - \Delta T)/T_0 \approx 1$ , the equation ends up taking a linear form that mimics the Clausius–Clapeyron equation for melting point. This approximation requires that the reference freezing temperature  $T_0$  be large compared to the temperature shift caused by the pressure change. In this study, the largest value we encounter is  $(T_0 - \Delta T)/T_0 = 1.03$ .

We have identified that the density anomaly  $\Delta\nu_{ls}$  is a key factor in determining the shape of the melting point line and also influences the change in Gibbs free energy barrier with pressure through its impact on  $\Delta\mu$ . Given that the ML-mW model exhibits a density anomaly roughly 230% larger than that of the mW model, our expectation is that decreasing pressure will have a much more significant influence on the nucleation rate in the ML-mW model over the mW model. When comparing our results for the two models, we do indeed observe that the slope  $(dP/dT)_{J=const}$  is larger for the ML-mW model. As shown in Fig. 4, the ML-mW model shows a larger increase in homogeneous nucleation rate coefficient for the same decrease of pressure. This analysis leads to our conclusion that the improved density anomaly makes ML-mW better equipped for studying ice nucleation in the context of changing pressures. When using a water model with a small density anomaly compared to real water, one may not capture the effects of pressure change on ice nucleation that would be exhibited in real water. A table of  $\Delta\nu_{ls}$  values for each model at negative pressures can be found in A.

Next we wish to compare the simulation results with Eq. 1. For reference values  $p_0$  and  $T_0$ , we use the temperature corresponding to  $J = 10^{32} \text{ m}^{-3} \text{ s}^{-1}$  at 1 atm, obtained from our constant cooling rate simulations. We input into Eq. 1 the values we obtained for  $T_m$  and  $\Delta\nu_{ls}$ , and the value for  $l_f$  that is published in Chan et al. at 1 atm [14]. Eq. 1 can then be used to predict the line of constant  $J = 10^{32} \text{ m}^{-3} \text{ s}^{-1}$  at negative pressures. The dashed lines in Fig. 4 show the resulting expressions plotted along with the simulation results, showing satisfactory agreement in the pressure regime of interest. We find that this simple linear approximation gives reliable estimates of freezing point elevation under negative pressures in this pressure range. We note that the contours in Fig. 3 are roughly linear as well, indicating that this trend remains consistent for smaller nucleation rate coefficients and lower supercooling.

Despite the various ways that the Gibbs free energy barrier is affected by decreasing pressures, our simulation results indicate that a linear approximation for the slope of constant nucleation rate lines can provide an excellent first order approximation in the pressure range that is studied in this work. The slope given in Eq. 1 is parallel to the melting point line, despite the fact that the elevated melting temperature is known to not be the only mechanism contributing the shape of constant nucleation rate lines. For example, previous molecular dynamics studies have observed that  $\gamma_{ls}$  increases in response to strongly positive pressures, dominating the trend in  $G^*$  and causing lines of constant nucleation rate to differ significantly in slope from that of the melting point line [37]. As seen in Fig. 4, we have observed that, within our error bounds, lines of constant nucleation rate are roughly parallel to the melting point line. The derivation of Eq. 1 assumes that  $\gamma_{ls}$  remains constant along lines of constant nucleation rate. The agreement between Eq. 1 and our data suggests that this approximation is valid in this range of pressures, for these models. Given that  $\gamma_{ls}$  is cubed in Eq. 2, it is likely to be a primary source of error in our linear approximation. However, since  $\gamma_{ls}$  decreases with both temperature and pressure, it is expected

that those two effects will tend to compensate for each other along lines of constant  $J$ , mitigating the error introduced in the approximation.

Furthermore, the derivation of Eq. 1 assumes that several thermodynamic values (interfacial energy  $\gamma_{ls}$ , enthalpy of fusion  $l_f$ , and kinetic flux) remain constant along lines of constant  $J$ . Despite experimental and theoretical uncertainty around the pressure dependence of these variables, we have shown that approximating these variables as constants results in satisfactory agreement with simulation results. It is possible that some of these variables increase along lines of constant  $J$  while others decrease, resulting in fortuitous cancellation of errors.

The finding that the enhancement in nucleation rate due to negative pressure can be approximated by Eq. 1 will be helpful in future studies of ice nucleation at negative pressures, and in designing laboratory experiments to further explore this phenomenon. An important result is that pressure and temperature can each be modified independently to achieve a given nucleation rate enhancement. The apparent equivalence between temperature and pressure in influencing nucleation rates is a useful perspective in studying atmospheric ice nucleation, for which focus has been placed primarily on the effect of temperature on nucleation rates with pressure held constant. This work provides further tools for the continued investigation of pressure fluctuations as an ice nucleation mechanism.

#### 4. Conclusion

We use MD simulation to evaluate homogeneous ice nucleation rate coefficients in a range of negative pressures, by means of constant cooling rate simulations as well as forward flux sampling. We compare the effect of negative pressure on nucleation rate coefficients between the ML-mW and the original mW model, concluding that the density difference between water and ice is a dominant factor in determining the extent to which nucleation rates in these models are increased when negative pressure (stress) is applied to the system. Based on this analysis, the ML-mW model is more appropriate than the original mW model for simulations involving ice nucleation at different pressures.

We obtain freezing temperature distributions for both water models at each pressure, which are then converted to nucleation rate coefficients. Contours of constant nucleation rate coefficient in pressure–temperature coordinates verify that a linear approximation can be used to predict the enhancement in nucleation rate due to negative pressure in the pressure range that is studied.

#### Declaration of Competing Interest

The authors declare that they have no known competing financial interests or personal relationships that could have appeared to influence the work reported in this paper.

#### Acknowledgments

Research reported in this publication was supported in part by funding provided by the National Aeronautics and Space Administration (NASA), under award number 80NSSC20M0124, Michigan Space Grant Consortium (MSGC). Funding from NSF grants AGS-1541998 and AGS-2019649 is gratefully acknowledged. Li acknowledges the support by NSF through award CBET-2053330. The High-Performance Computing Shared Facility (Portage) at Michigan Technological University was used in obtaining results presented in this publication. We are grateful to Prof. Issei Nakamura and the LAMMPS community for helpful discussions.

## Appendix A. Determination of $\Delta v_{ls}$ , Freezing Temperatures, and Melting Temperatures

### A.1. Freezing temperature

**Fig. 5** is an example evolution of the  $N_{ice}/N_{total}$  ratio for one constant cooling ramp simulation run. The figure shows the raw data, the sigmoidal fit, and the nominal freezing temperature of the run as described in the Methods section. Note added in proof: In the process of making final checks we identified an inconsistency in the molecular mass of water used in the simulations. In these constant cooling simulations the mass was 18.15 g/mole, whereas in all other calculations 18.015 g/mole was used. We have run ten constant cooling realizations at atmospheric pressure and at -500 atmospheres using a mass of 18.015 g/mole, and find that the mean freezing temperature and nucleation rate coefficients vary well within the statistical uncertainties. The findings presented in the paper therefore are not influenced by this inconsistency.

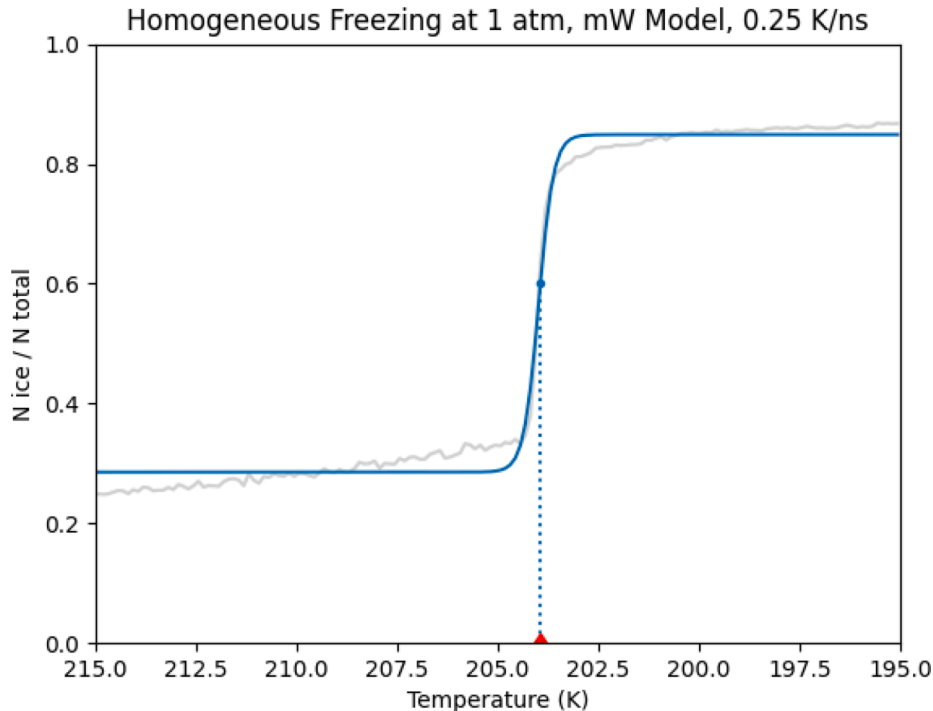


**Fig. 5.** An example of one freezing trajectory at 1 atm. The grey line shows the raw data of ice fraction. The colored line is a sigmoid fit to the data. The blue dot indicates the inflection points that is used as the nominal freezing temperature for the run. The dashed line and red marker are a guide for the eye.

### A.2. Melting temperature

The data points for the mW and ML-mW melting points in **Fig. 4** are obtained by using the direct-phase coexistence method at each pressure, where the melting temperature is taken as the lowest temperature where the system completely melts [26] [27]. **Fig. 6** shows our results at 1 atm for the two water models. We can use our 1 atm result as validation. While our outcome for the mW model precisely matches published results of 273 K, we find that our outcome for ML-mW (292 K) is different from the published value by Chan et al. [14] for the melting temperature of ML-mW (289 K). Chan et al. [14] used a different method than used here, but other work has shown that these two methods typically agree [38], so the discrepancy is at this point unexplained. Nevertheless, for this study we are not concerned with the exact value of the melting point, but the relative changes with respect to pressure, and the qualitative behavior of the freezing point relative to the melting point.

The results for melting temperatures are summarised in **Table 1**. The uncertainty on the reported values are  $\pm 1$ K.

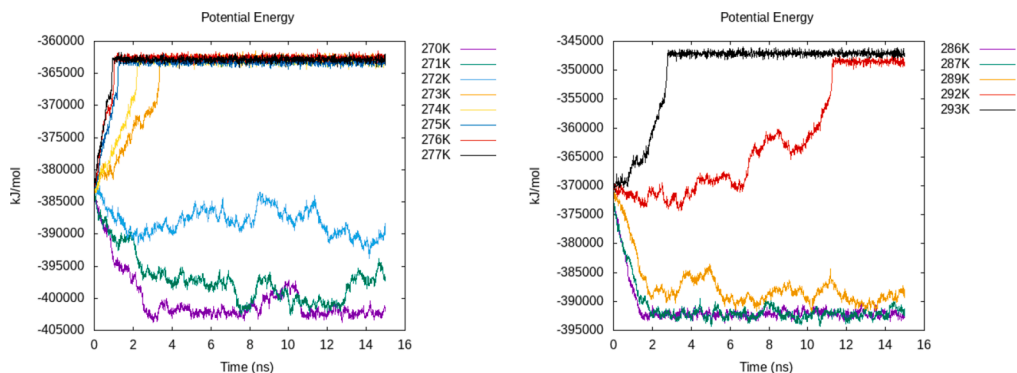


**Fig. 6.** Left: Original mW model potential energy trajectories at 1 atm, showing the system melting at temperatures equal or greater than 273 K. Right: ML-mW model potential energy trajectories at 1 atm, showing the system melting at temperatures equal or greater than 292 K.

**Table 1**

Melting temperatures of ML-mW model and original mW model at negative pressures.

Pressure (atm)	ML-mW (K)	mW (K)	Experiment (K)
1	292	273	273
-500	295	274	
-1000	298	275	279 [9]

**A.3. Density anomaly  $\Delta v_{ls}$** 

[Table 2](#) reports  $\Delta v_{ls}$  values that we have computed for the mW and ML-mW models at their equilibrium melting temperatures at 1 atm, -500 atm, and -1000 atm. The values were determined by measuring the molar volume ( $\text{cm}^3 \text{mol}^{-1}$ ) of an equilibrated box of liquid containing  $\sim 4100$  water molecules and separately measuring the molar volume of equilibrated ice at the same temperature and pressure. We take the difference between these values to obtain  $\Delta v_{ls}$ . The values we report at 1 atm are in agreement with published values in Chan et al. [14].

**Table 2** $\Delta v_{ls}$  ( $\text{cm}^3 \text{mol}^{-1}$ ) at liquid-solid coexistence temperature for ML-mW model and original mW model at negative pressures.

Pressure (atm)	ML-mW	mW	Experiment
1	-1.35	-0.42	-1.61 [14]
-500	-1.17	-0.35	
-1000	-0.95	-0.27	

**Appendix B. Convergence and validation of FFS**

To validate the convergence of FFS calculation with respect to the number of configurations ( $N_i$ ) collected at each interface  $\lambda_i$ , we repeat FFS calculations under two conditions, *i.e.*, 227 K, -500 atm and 233 K, 1 atm, by collecting 1,000 configurations at each interface. The calculated rates are compared against with those computed using 600 configurations, based on three independent FFS runs each collecting 200 configurations. As shown in [Table 3](#), the calculated rates are virtually unchanged with respect to the number of collected configurations, demonstrating the convergence of rate constants calculated by FFS.

The validity of FFS can be further confirmed by explicitly comparing the rates obtained by different approaches under a condition where spontaneous nucleation becomes accessible to direct MD. Here we choose such condition to be 227 K, -500 atm, guided by the calculated ice nucleation rate based on FFS. We carry out 20 independent direct MD simulations using an isobaric-isothermal canonical ensemble, each lasting one micro second. From the distribution of induction time to ice nucleation ( $t_{\text{ind}}$ ), defined as the time taken to form a critical ice nucleus, we obtain the distribution of probability for the system remaining liquid  $P_{\text{liq}}(t)$ . Following the procedure described in Cox et al. [34], we fit the calculated  $P_{\text{liq}}(t)$  by the following equation:

$$P_{\text{liq}}(t) = \exp[-(Rt)^\gamma], \quad (\text{B.1})$$

where  $R$  is nucleation rate and  $\gamma$  is fitting constant, as shown in [Fig. 7](#). The fitted ice nucleation rate  $R$  for this condition is found to agree well with the FFS calculations, as shown in [Table 3](#), thus further confirming the validity of our FFS study.

**Table 3**Comparison of the calculated ice nucleation rates ( $\text{m}^{-3} \text{s}^{-1}$ ).

Method	227 K, -500 atm	233 K, 1 atm
FFS (600 configurations)	$3.72 \pm 0.97 \times 10^{31}$	$3.00 \pm 0.43 \times 10^{26}$
FFS (1,000 configurations)	$3.07 \pm 1.5 \times 10^{31}$	$1.54 \pm 0.62 \times 10^{26}$
Direct MD (20 runs)	$6.93 \pm 0.13 \times 10^{31}$	N/A

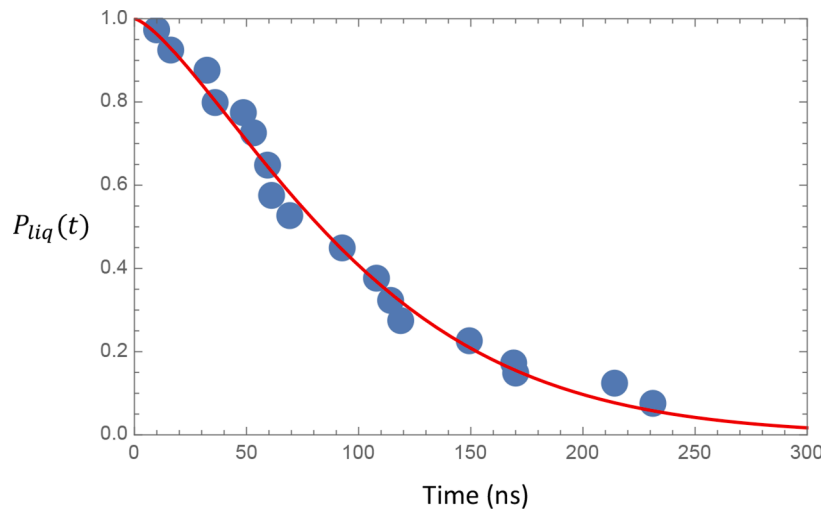


**Fig. 7.** Ice nucleation rate  $R$  is obtained by fitting the calculated  $P_{liq}(t)$  (blue dots) by Eqn. B.1. The fitted distribution is represented by the red line.

### Appendix C. Derivation of $p(T)$ Approximation

When the pressure of water is decreased, the nucleation rate is lowered due to a change in the chemical potential difference between liquid water and ice. Deriving a pressure-dependent formulation of the chemical potential difference between ice and liquid water under isothermal conditions, Némec 2013 arrives at the following expression [35]:

$$\mu_s - \mu_l = (p - p_{e,s})v_s - (p - p_{e,l})\frac{v_l(p) + v_l(p_{e,l})}{2} - kT \ln \left( \frac{p_{e,l}}{p_{e,s}} \right). \quad (\text{C.1})$$

The derivation can be found in Eqs. 2–5 of Némec 2013 [35]. The value of  $\mu_s - \mu_l$  that is obtained is for the given pressure  $p$ . The molecular volumes ( $\text{m}^3$ ) for ice and liquid water are denoted by  $v_s$  and  $v_l$ . Note that in the present work, we use molar volumes ( $\text{cm}^3 \text{ mol}^{-1}$ ). Eq. C.1 is derived in reference to known values for  $\mu_s$  and  $\mu_l$  at their equilibrium vapor pressures  $p_{e,s}$  and  $p_{e,l}$  respectively. This reference value is given as the third term on the right hand side of the equation, with the preceding terms interpreted as a change due to pressure. We substitute the ratio of equilibrium vapor pressures over supercooled liquid and ice with the commonly used expression from the Clausius–Clapeyron equation

$$\frac{p_{e,l}}{p_{e,s}} = \exp \left( \frac{l_f}{RT_m} \frac{(T_m - T)}{T} \right). \quad (\text{C.2})$$

We also impose the assumption that  $(p - p_{e,s}) \approx (p - p_{e,l})$ . This is valid because the values of  $p$  that we are investigating are on the order or 10–100 MPa, many orders of magnitude larger than the maximum difference  $p_{e,l} - p_{e,s}$  seen in water (roughly  $3 \times 10^{-5}$  MPa). This approximation, combined with the substitution of Eq. C.2 gives us the following form, now expressed in terms of moles instead of per molecule:

$$\mu_s - \mu_l = (p - p_{e,l}) \left[ (v_s - v_l(p_{e,l})) - \frac{1}{2}(v_l(p) - v_l(p_{e,l})) \right] - \frac{l_f(T_m - T)}{T_m}. \quad (\text{C.3})$$

From here we shall make some adjustments to the equation to suit our needs. First, we identify  $p_{e,l}$  to be our reference pressure  $p_0$ , and  $\Delta p = p - p_0$ . We substitute  $\Delta v_{ls} = v_l(p_0) - v_s$  and define  $\Delta\mu = \mu_l - \mu_s$ :

$$\Delta\mu = \Delta p \left( \Delta v_{ls} + \frac{1}{2}(v_l(p) - v_l(p_0)) \right) + \frac{l_f(T_m - T)}{T_m}. \quad (\text{C.4})$$

Lastly, we make the approximation that  $\frac{1}{2}(v_l(p) - v_l(p_0)) \approx 0$ . In other words, we make the assumption that  $v_l$  is a constant, independent of pressure. In actuality, the value of  $v_l$  increases as the pressure decreases, due to water becoming less dense and closer in density to ice. This pressure dependence in  $v_l$  may explain the slight nonlinearity of temperature–pressure contours in Fig. 3. To better approximate the observations, the  $v_l(p) - v_l(p_0)$  term needs to be kept. To reasonable approximation we can ignore this dependence. Thus we arrive at Eq. 3 of this work, an approximation for the difference in chemical potential between supercooled liquid and solid, accounting for a pressure change:

$$\Delta\mu = \frac{l_f(T_m - T)}{T_m} + \Delta p \Delta v_{ls}. \quad (\text{C.5})$$

This relation works well when  $T$  is close to  $T_m$  and the temperature dependence of  $l_f$  can be neglected. Higher order terms should be included when  $T$  is much lower than  $T_m$ . The chemical potential contributes to the Gibbs free energy barrier to nucleation, and the nucleation rate coefficient can be written as

$$J = A \exp\left(\frac{C}{T \Delta \mu^2}\right), \quad (C.6)$$

with  $C = 16\pi\gamma_{ls}^3/(3k_B\rho^2)$ . In this derivation, we assume that surface tension ( $\gamma_{ls}$ ), density ( $\rho$ ), and kinetic prefactor ( $A$ ) remain constant for small changes in temperature and pressure. Starting from reference point  $J(p_0, T_0)$ , we aim to find an expression for lines of constant nucleation rate in temperature-pressure coordinates:

$$J(p_0 + \Delta p, T_0 + \Delta T) = J(p_0, T_0). \quad (C.7)$$

We use Eqs. C.5 and C.6 in the above expression to solve for the slope ( $\Delta p/\Delta T$ ) of the constant nucleation rate lines. Because we have taken  $A$  and all terms in  $C$  to be constant, they are eliminated from both sides of the expression. Taking the logarithm of both sides, we have

$$(T_0 + \Delta T) \left( \frac{l_f(T_m - T_0 - \Delta T)}{T_m} + \Delta p \Delta v_{ls} \right)^2 = T_0 \left( \frac{l_f(T_m - T_0)}{T_m} \right)^2. \quad (C.8)$$

Next we divide both sides by  $T_0$  and make the approximation that  $(T_0 - \Delta T)/T_0 \approx 1$ . After taking the square root of both sides and rearranging, the resulting relation is

$$\frac{\Delta p}{\Delta T} = \frac{l_f}{T_m \Delta v_{ls}} \quad (C.9)$$

Using  $\Delta p = p - p_0$  and  $\Delta T = T - T_0$ , we can express the relation as

$$p(T) = p_0 + \frac{l_f}{T_m \Delta v_{ls}} (T - T_0)$$

Overall, the derivation is valid in the regime of linear response where the change of  $T$  or  $p$  is small and can be considered as small perturbation. It may also work in a greater range of  $(T, p)$  change, depending on the linearity of the melting line.

## References

- [1] N. Maeda, Brief overview of ice nucleation, *Molecules* 26 (2) (2021) 392.
- [2] B. Murray, D. O'sullivan, J. Atkinson, M. Webb, Ice nucleation by particles immersed in supercooled cloud droplets, *Chem. Soc. Rev.* 41 (19) (2012) 6519–6554.
- [3] N.E. Dorsey, The freezing of supercooled water, *Trans. Am. Philos. Soc.* 38 (3) (1948) 247–328.
- [4] S. Nalesto, M.J. Bussemaker, R.P. Sear, M. Hodnett, J. Lee, A review on possible mechanisms of sonocrystallisation in solution, *Ultrason. Sonochem.* 57 (2019) 125–138.
- [5] F. Yang, R.A. Shaw, C.W. Gurganus, S.K. Chong, Y.K. Yap, Ice nucleation at the contact line triggered by transient electrowetting fields, *Appl. Phys. Lett.* 107 (2015) 264101.
- [6] J. Niehaus, W. Cantrell, Contact freezing of water by salts, *J. Phys. Chem. Lett.* 6 (2015) 3490–3495.
- [7] F. Yang, O. Cruikshank, W. He, A. Kostinski, R. Shaw, Nonthermal ice nucleation observed at distorted contact lines of supercooled water drops, *Phys. Rev. E* 97 (2018) 023103.
- [8] E. Roedder, Metastable superheated ice in liquid-water inclusions under high negative pressure, *Science* 155 (3768) (1967) 1413–1417.
- [9] C. Marcolla, Ice nucleation triggered by negative pressure, *Scient. Rep.* 7 (2017).
- [10] F. Yang, W.H. Cantrell, A.B. Kostinski, R.A. Shaw, A.M. Vogelmann, Is contact nucleation caused by pressure perturbation? *Atmosphere* 11 (1) (2020).
- [11] T. Li, D. Donadio, G. Galli, Ice nucleation at the nanoscale probes no man's land of water, *Nat. Commun.* 1887 (2013).
- [12] V. Bianco, P.M. de Higes, C.P. Lamas, E. Sanz, C. Vega, Anomalous behavior in the nucleation of ice at negative pressures, *Phys. Rev. Lett.* 126 (2021) 015704.
- [13] V. Molinero, E. Moore, Water modeled as an intermediate element between carbon and silicon, *J. Phys. Chem. B* 113 (2009) 4008–4016.
- [14] H. Chan, M.J. Cherukara, B. Narayanan, T.D. Loeffler, C. Benmore, S.K. Gray, S.K. R.S. Sankaranarayanan, Machine learning coarse grained models for water, *Nat. Commun.* 10 (2019) 2009–2014.
- [15] R.J. Allen, D. Frenkel, P.R. Ten Wolde, Simulating rare events in equilibrium or nonequilibrium stochastic systems, *J. Chem. Phys.* 124 (2) (2006) 024102.
- [16] J.R. Espinosa, E. Sanz, C. Valeriani, C. Vega, Homogeneous ice nucleation evaluated for several water models, *J. Chem. Phys.* 141 (2014) 18C529.
- [17] S. Plimpton, Fast Parallel Algorithms for Short-Range Molecular Dynamics, *J. Comput. Phys.* 117 (1) (1995) 1–19.
- [18] J.C. Johnston, V. Molinero, Crystallization, melting, and structure of water nanoparticles at atmospherically relevant temperatures, *J. Am. Chem. Soc.* 134 (15) (2012) 6650–6659, <https://doi.org/10.1021/ja210878c>.
- [19] P.J. Steinhardt, D.R. Nelson, M. Ronchetti, Bond-orientational order in liquids and glasses, *Phys. Rev. B* 28 (1983) 784–805.
- [20] L. Lupi, A. Hudait, V. Molinero, Heterogeneous nucleation of ice on carbon surfaces, *J. Am. Chem. Soc.* 136 (2014) 3156–3164.
- [21] B. Zobrist, T. Koop, B.P. Luo, C. Marcolla, T. Peter, Heterogeneous ice nucleation rate coefficient of water droplets coated by a nonadecanol monolayer, *J. Phys. Chem. C* 111 (5) (2007) 2149–2155, <https://doi.org/10.1021/jp066080w>.
- [22] A.F. Heneghan, A.D.J. Haymet, Liquid-to-crystal nucleation: A new generation lag-time apparatus, *J. Chem. Phys.* 117 (11) (2002) 5319–5327, <https://doi.org/10.1063/1.1497635>.
- [23] R.A. Shaw, A.J. Durant, Y. Mi, Heterogeneous surface crystallization observed in undercooled water, *J. Phys. Chem. B* 109 (20) (2005) 9865–9868, <https://doi.org/10.1021/jp0506336>.
- [24] H. Kanno, R.J. Speedy, C.A. Angell, Supercooling of water to -92 °C under pressure, *Science* 189 (4206) (1975) 880–881.
- [25] T. Koop, B. Luo, U.M. Biermann, P.J. Crutzen, T. Peter, Freezing of hno3/h2so4/h2o solutions at stratospheric temperatures: Nucleation statistics and experiments, *J. Phys. Chem. A* 101 (1997) 1117–1133.
- [26] J.R. Espinosa, E. Sanz, C. Valeriani, C. Vega, On fluid-solid direct coexistence simulations: The pseudo-hard sphere model, *J. Chem. Phys.* 139 (2013) 144502.
- [27] R. García Fernández, J.L.F. Abascal, C. Vega, The melting point of ice Ih for common water models calculated from direct coexistence of the solid-liquid interface, *J. Chem. Phys.* 124 (2006) 144506.
- [28] T. Li, D. Donadio, G. Russo, G. Galli, Homogeneous ice nucleation from supercooled water, *Phys. Chem. Chem. Phys.* 13 (44) (2011) 19807–19813.
- [29] A. Haji-Akbari, R.S. DeFever, S. Sarupria, P.G. Debenedetti, Suppression of subsurface freezing in free-standing thin films of a coarse-grained model of water, *Phys. Chem. Chem. Phys.* 16 (47) (2014) 25916–25927.

- [30] A. Haji-Akbari, P.G. Debenedetti, Direct calculation of ice homogeneous nucleation rate for a molecular model of water, *Proc. Natl. Acad. Sci. USA* 112 (34) (2015) 10582–10588.
- [31] R. Cabriolu, T. Li, Ice nucleation on carbon surface supports the classical theory for heterogeneous nucleation, *Phys. Rev. E* 91 (2015) 052402.
- [32] L. Lupi, B. Peters, V. Molinero, Pre-ordering of interfacial water in the pathway of heterogeneous ice nucleation does not lead to a two-step crystallization mechanism, *J. Chem. Phys.* 145 (21) (2016) 211910.
- [33] L. Lupi, A. Hudait, B. Peters, M. Grünwald, R.G. Mullen, A.H. Nguyen, V. Molinero, Role of stacking disorder in ice nucleation, *Nature* 551 (7679) (2017) 218–222.
- [34] S.J. Cox, S.M. Kathmann, B. Slater, A. Michaelides, Molecular simulations of heterogeneous ice nucleation. i. controlling ice nucleation through surface hydrophilicity, *J. Chem. Phys.* 142 (18) (2015) 184704, <https://doi.org/10.1063/1.4919714>.
- [35] T. Némec, Estimation of ice–water interfacial energy based on pressure-dependent formulation of classical nucleation theory, *Chem. Phys. Lett.* 583 (2013) 64–68.
- [36] J. Huang, L.S. Bartell, Kinetics of homogeneous nucleation in the freezing of large water clusters, *J. Phys. Chem.* 99 (12) (1995) 3924–3931.
- [37] J.R. Espinosa, A. Zaragoza, P. Rosales-Pelaez, C. Navarro, C. Valeriani, C. Vega, E. Sanz, Interfacial free energy as the key to the pressure-induced deceleration of ice nucleation, *Phys. Rev. Lett.* 117 (2016) 135702, <https://doi.org/10.1103/PhysRevLett.117.135702>.
- [38] C. Vega, E. Sanz, J.L.F. Abascal, E.G. Noya, Determination of phase diagrams via computer simulation: methodology and applications to water, electrolytes and proteins, *J. Phys.: Condens. Matter* 20 (15) (2008) 153101, <https://doi.org/10.1088/0953-8984/20/15/153101>.